Ripple phase formation in phosphatidylcholine: Effect of acyl chain relative length, position, and unsaturation

Beth A. Cunningham,[1] Ari-David Brown,[1] David H. Wolfe,[2] W. Patrick Williams,[3] and Anthony Brain[3]
[1]*Physics Department, Bucknell University, Lewisburg, Pennsylvania 17837*
[2]*Astronomy & Physics Department, Lycoming College, Williamsport, Pennsylvania 17701*
[3]*Life Sciences Division, King's College London, Campden Hill Road, London W8 7AH, United Kingdom*
(Received 11 February 1998)

The ripple phases of a range of mixed-acid phosphatidylcholine derivatives with one saturated C_{18} chain and the other chain of variable length or unsaturation were studied using differential scanning calorimetry, x-ray diffraction, and freeze-fracture electron microscopy. The temperature dependences of their ripple wavelength (λ), stacking repeat distance (d_s), and the monoclinic angle θ_m defining their unit cell were measured and found to be consistent with an inherently asymmetric ripple phase with an amplitude that slowly increases with temperature. The temperature spans of the ripple phases of the saturated mixed-chain derivatives and the derivatives containing unsaturated chains were found to be larger and smaller, respectively, than those of homoacyl derivatives of the same equivalent chain length. This was shown to be consistent with the sliding-chain model proposed by Cevc (Biochemistry 30, 7186–7197, 1991). The tendency of phosphatidylcholine derivatives to form asymmetric ripple phases and the possible molecular organization of such phases are discussed in terms of different models. X-ray diffraction evidence was found for the existence of a secondary ripple phase with a wavelength about 1.8 times greater than the conventional pretransition ripple phase. This phase is formed in samples freshly cooled from the liquid-crystal phase and tends to persist longer than the conventional ripple phase on cooling to the gel phase. Freeze-fracture electron microscopy suggests that it is symmetric in cross section possibly reflecting the interaction of two opposing pretransition ripples.
[S1063-651X(98)12209-2]

PACS number(s): 87.15.−v, 64.70.Md, 61.30.Eb

INTRODUCTION

Hydrated samples of fully saturated phosphatidylcholine (PC) derivatives normally exist in one of four bilayer phases: a crystalline (L_c) phase formed on equilibration at low temperatures in which the acyl chains are packed on an orthorhombic lattice; a gel ($L_{\beta'}$) phase in which the fully extended acyl chains, packed on a quasihexagonal lattice, are tilted with respect to the bilayer normal; a ripple ($P_{\beta'}$) phase in which the lipid bilayer is distorted by a periodic ripple characterized by a two-dimensional monoclinic lattice; and a conventional liquid-crystal (L_α) phase in which the acyl chains are melted [1].

The existence of a ripple phase, in particular, has been a source of considerable interest to a broad range of researchers for many years. The majority of reports on the ripple phase relate to homoacyl disaturated PC derivatives. Ripple phases are, however, also formed in saturated mixed-chain PC derivatives [2,3] and in some derivatives containing unsaturated chains [4,5 and this paper]. They are found in mixtures of PC with cholesterol [6,7] and even occasionally in other lipid systems such as phosphatidylglycerols [8] and substituted phosphatidylethanolamines [9].

The structure of the ripple phase has been extensively studied using x-ray diffraction [2,3,10–20], neutron diffraction [6], freeze-fracture electron microscopy [21–26], and scanning-tunneling microscopy [27,28].

Freeze-fracture techniques have revealed the existence of a large number of different ripple profiles. The predominant ripple form found in pure PC systems is asymmetric with a sawtooth cross section and a wavelength of about 12–16 nm [25,26]. Lipid mixtures, however, are often characterized by a symmetrical ripple often referred to as a macroripple, which has a wavelength approximately double that of the pretransition ripple [29]. Small areas of macroripple and of other types of ripple of different symmetry and wavelength also occur in pure PC dispersions. The structure of these alternative ripple forms is still a matter of some debate but can in many cases be explained in terms of summations and/or interactions of the basic pretransition ripple [26].

Electron density distributions calculated by Wack and Webb [16] confirm the basic asymmetry of the pretransition ripples. Recent calculations performed by Sun *et al.* [20] indicate that the bilayer thicknesses in the two sides of the sawtooth are appreciably different. They estimate a bilayer thickness of 3.8 and 3.1 nm, respectively, for the long and short sides of the ripple for di-14:0 PC [30] and suggest that the ripple consists of alternating sections of lipid of gel and liquid-crystal-like phase character.

Many theoretical models have been put forward in attempts to explain the formation of the ripple phase. In general, they are divided into two groups: those based on purely thermodynamic considerations [31–37] and those based on a statistical mechanical approach [38–43]. Excellent summaries of the ideas underlying these models can be found in Carlson and Sethna [34] and Scott and McCullogh [44].

While such models have a valuable role in exploring possible explanations of the factors underlying ripple phase formation, the number of assumptions and simplifications required to make them mathematically handlable means that they have limited predictive value. Cevc [45] has adopted a

rather different approach and has developed a phenomenological model based on the idea that ripple formation is associated with a sliding of the lipid molecules along their longitudinal axes leading to an increased exposure of the lipid headgroups to the hydrophilic medium. The model provides useful equations for the prediction of the ($L_{\beta'} \rightarrow P_{\beta'}$) and ($P_{\beta'} \rightarrow L_{\alpha}$) phase transition temperatures but runs into similar problems when it comes to explaining the inherent anisotropy of the ripple profile.

In an attempt to examine the driving forces of the ripple phase transition further, we have studied the occurrence of the ripple phase in fully hydrated dispersions of a range of mixed-acid PC derivatives with one saturated C_{18} chain and the other chain of variable length or unsaturation, using differential scanning calorimetry (DSC), x-ray diffraction, and freeze-fracture electron microscopy. We were particularly interested in the temperature ranges of the different ripple phases and general organization of the ripple phase and the chain packing of the lipids as reflected in small-angle x-ray diffraction (SAXS) and wide-angle x-ray diffraction (WAXS) measurements, respectively. The x-ray studies performed on fully hydrated samples suggested that the ripple structures present in our fully hydrated samples were mainly of the standard pretransition type. Evidence of the formation of appreciable amounts of a ripple phase with a wavelength approximately double that of the pretransition ripple was, however, found in a partially hydrated sample of one of the lipids.

MATERIALS AND METHODS

Lipids. All phospholipids were obtained from Avanti Polar Lipids, Inc. (Alabaster, AL) and used without further purification.

Calorimetry. Calorimetric measurements were performed using a Perkin-Elmer DSC-2 scanning calorimeter fitted with a subambient accessory. Aqueous dispersions (usually 1:1 w/w) were prepared by direct addition of distilled water to the lipid powder and hermetically sealed in aluminum pans. All samples were heated over a temperature range of at least 50 °C and thermograms were recorded on heating and cooling at a rate of 5 °C/min. At least three heating/cooling cycles on two separate samples were performed. Onset temperatures were taken to be at the departure of the rising endotherm from the baseline. The system was calibrated using the known thermal parameters for the melting of indium and/or cyclohexane.

X-ray diffraction. Samples were prepared by resuspending weighed amounts of lipid in distilled water. The resulting dispersions were then heated above their main phase transition and subjected to at least three freeze/thaw cycles. The 18:0, 18:2 lipid dispersion was prepared, as far as was practical, in a N_2-filled glove box to minimize the chances of lipid oxidation. Following hydration, the samples were stored at −20 °C for approximately 24 h before examination.

Real-time x-ray diffraction studies were performed using a monochromatic (0.154 nm) focused x-ray beam at Station 8.2 of the SERC Daresbury Synchrotron Facility, UK, using a purpose-built SAXS/WAXS camera. Detailed descriptions of the measuring system have been published elsewhere [46,47]. The data-acquisition system allowed the collection of 255 consecutive 5 s diffraction patterns with an intervening 10 μs wait-time. The SAXS detector was calibrated using at least the first nine orders of wet rat tail collagen (repeat distance of 67.0 nm). The WAXS detector was calibrated using the peaks arising from hexagonal crystalline ice [48] formed in frozen samples as an internal standard.

Freeze-fracture electron microscopy. Lipid samples were thermally quenched from subambient temperatures using a purpose-built temperature equilibration system [49]. Following thermal quenching, the sample was transferred to a Polaron freeze-fracture device for processing. The resulting replicas were examined using a Philips EM301G electron microscope.

RESULTS

Differential scanning calorimetry

DSC measurements were performed on fully hydrated samples of mixed-chain PC derivatives with one C_{18} chain and the other chain variable in length and/or unsaturation. All samples were incubated for at least 5 min above the main transition temperature just prior to measurement in order to eliminate complications associated with the possible formation of crystal (L_c) phases. Typical DSC heating thermograms for di-18:0 PC, 18:0,16:0 PC, 16:0,18:0 PC, 18:0,14:0 PC, 18:0,18:1 PC, 18:1,18:0 PC, and 18:0,18:2 PC are presented in Fig. 1(a). The corresponding cooling curves, measured immediately after the initial heating, are shown in Fig. 1(b). Di-18:0 PC and the saturated mixed-chain PC species (18:0,16:0 PC, 16:0,18:0 PC, and 18:0,14:0 PC) all exhibit an ($L_{\beta'} \rightarrow P_{\beta'}$) pretransition and a main ($P_{\beta'} \rightarrow L_{\alpha}$) transition on heating. In the case of di-18:0 PC, the pretransition was also seen on cooling but only the main transition was seen under these conditions for the mixed-chain species.

No pretransition was observed, either on heating or cooling, for the PC species 18:0,18:1 PC, 18:1,18:0 PC, and 18:0,18:2 PC containing unsaturated acyl chains. In order to check that any possible pretransition was not being masked by the large endotherm associated with ice melting, these measurements were repeated on supercooled samples. The samples were first cooled to around −15 °C and then reheated while still in the supercooled state. Only a single peak, corresponding to the main lipid transition, was observed. No indication of the occurrence of a pretransition in either the cooling or heating traces was found under our measuring conditions.

The collected values for the temperatures and molar enthalpies of the ($L_{\beta'} \rightarrow P_{\beta'}$) and ($P_{\beta'} \rightarrow L_{\alpha}$) transitions observed in this study are presented in Table I. The values of the transition temperatures for di-18:0 PC and fully saturated mixed-acyl chain PC derivatives are in good agreement with previously published values ([3,50,51], and references therein). The enthalpies, while in general agreement with previously published values, are somewhat variable probably reflecting the requirement to cycle the samples under conditions in which the formation of the crystalline phase was inhibited. Fewer measurements have been carried out on mixed-chain PC derivatives containing unsaturated chains but again our values are in good agreement with published values [52,53].

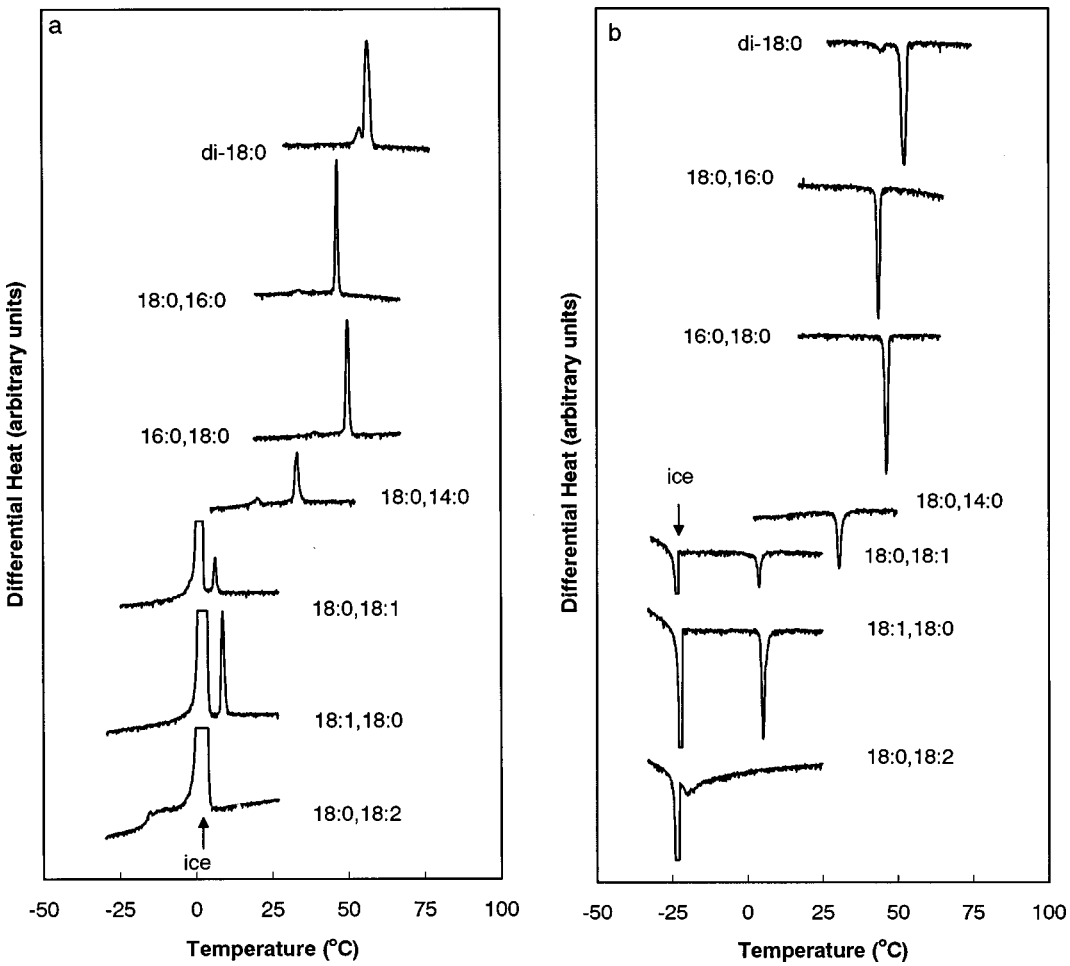

FIG. 1. DSC thermograms for the PC series di-18:0 PC, 18:0,16:0 PC, 16:0,18:0 PC, 18:0,14:0 PC, 18:0,18:1 PC, 18:1,18:0 PC, and 18:0,18:2 PC fully hydrated in water. (a) First heating scans; (b) subsequent cooling scans. The heating and cooling rates were 5 °C/min.

X-ray diffraction and freeze-fracture measurements

The structural properties of the ripple phase ($P_{\beta'}$) were examined using real-time SAXS/WAXS measurements and freeze-fracture electron microscopy. Attention was concentrated on three different aspects of the ripple phase: the properties of pretransition ripples in fully saturated molecular species; the occurrence of ripple phases in mixed-acyl chain systems containing unsaturated fatty acyl chains; and the formation of long-wavelength ripples.

Pretransition ripple phases in fully saturated molecular species. SAXS/WAXS measurements were carried out under conditions analogous to those employed in the DSC measurements. As anticipated, all the fully saturated lipids gave rise to well-defined ripple phases in their pretransition temperature ranges. In the case of x-ray measurements, however, the formation of such phases was seen both in heating and cooling scans. Examples of SAXS patterns of ripple phases for the different lipids, measured at temperatures corresponding to the center of their respective pretransition ranges, are presented in Fig. 2. In agreement with Tenchov *et al.* [15], we observed significant differences in the relative amplitudes of different ripple phase diffraction maxima in heating and cooling scans and all observations, unless otherwise stated, relate to heating scans.

TABLE I. Transition temperatures and enthalpies for a series of fully hydrated samples of mixed acid PC derivatives with one C_{18} chain and the other chain variable in length and/or unsaturation.

Lipid	T_p (°C)	ΔH_p (kJ/mol)	T_m (°C)	ΔH_m (kJ/mol)
di-18:0 PC	51.1	6.5	55.1	37.9
18:0,16:0 PC	29.0	9.9	45.1	24.0
16:0,18:0 PC	35.5	2.6	48.0	28.5
18:0,14:0 PC	17.5	6.9	31.2	33.4
18:0,18:1 PC			5.5	20.6
18;1,18:0 PC			7.4	23.7
18:0,18:2 PC			−17.3	11.0

All the lipids examined showed a small diffraction maximum at about 12.0 nm ($S=0.083\,\mathrm{nm}^{-1}$) and a prominent first-order stacking repeat at about 6.0 nm ($S=0.166\,\mathrm{nm}^{-1}$), corresponding to the (01) and (10) spacings of the ripple phase, together with a number of less prominent maxima arising from the cross terms of the ripple lattice and higher-order reflections from the stacking repeat. Following Wack and Webb [16], we have indexed these spectra in terms of a 2D monoclinic lattice characterized by a ripple wavelength λ, a stacking repeat distance d_s, and a monoclinic angle θ_m. Values for θ_m, d_s, and λ were determined by applying the monoclinic spacing formula

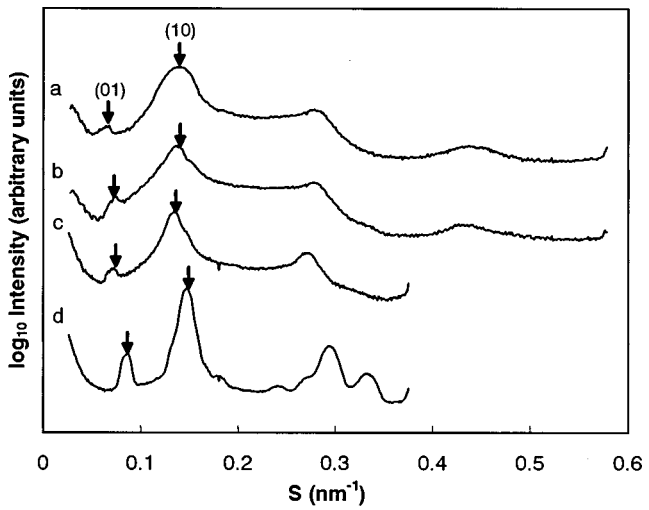

FIG. 2. SAXS diffraction patterns exhibiting the ripple phase in fully hydrated samples of (a) di-18:0 PC at 55.1 °C, (b) 18:0,16:0 PC at 43.3 °C, (c) 16:0,18:0 PC at 47.8 °C, (d) 18:0,14:0 PC at 27 °C. The positions of the (01) and (10) diffraction maxima are indicated by the arrows.

$$\frac{1}{d_{h,k}^2}=\frac{1}{\sin^2\theta_m}\left[h^2/d_s^2+k^2/\lambda^2-2hk\,\cos\,\theta_m/(d_s\lambda)\right] \quad (1)$$

to all the peaks simultaneously and minimizing the difference between the expected spacing for each peak and the experimentally determined spacings. Collected values for these parameters are presented in Table II. They are in good agreement with the values reported by Wack and Webb [16] for di-18:0 PC and Mattai *et al.* [3] for saturated mixed-chain lipids.

A detailed picture of the temperature-dependent changes in the SAXS pattern of 18:0,14:0 PC, taken as a representative lipid of this group, is presented in the form of a gray-level intensity plot in Fig. 3. The plot is constructed from data collected in a continuous series of 5 s frames measured

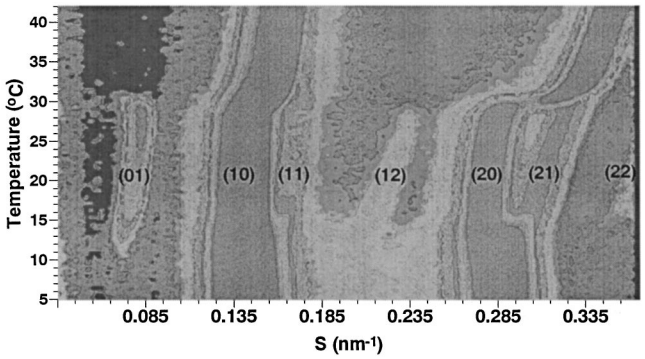

FIG. 3. Gray-level plot of x-ray scattering intensity as a function of temperature for fully hydrated 18:0,14:0 PC during a heating scan at a rate of 2 °C/min. The lighter areas represent higher intensities. The diffraction maxima of the ripple phase are indicated.

as the sample is heated from 5 to 42 °C at a rate of 2 °C/min. At 5 °C, the sample is in a lamellar phase characterised by first- (10) and second-order (20) maxima corresponding to a lamellar repeat distance of 6.58 nm. The (01) diffraction maximum of the ripple phase first starts to appear at about 11 °C and the (11), (12), (21), and (22) small-angle maxima are all clearly visible by 15 °C. The maxima associated with the ripple phase persist to about 30 °C, at which point they abruptly disappear, and the positions of the (10) and (20) maxima shift as the lamellar repeat distance decreases to 6.01 nm, signaling a transition to the L_α phase. Plots of the temperature dependences of θ_m, λ, and d_s for 18:0,14:0 PC during heating and cooling scans are presented in Fig. 4. The ripple wavelength λ, as illustrated in Fig. 4(a), showed a slow decrease on heating from about 12.6 nm at 17 °C to 11.8 nm at 29 °C, followed by a rapid increase to 13.0 nm at 32 °C. Essentially the reverse behavior was seen on cooling. Matuoka *et al.* [18] have reported similar changes in fully hydrated samples of di-14:0 PC. The initial decrease, and final increase, in λ with temperature almost certainly reflect the formation of the ripple phase from the flanking planar

TABLE II. Wide-angle diffraction spacings, bilayer repeat spacing, and ripple wavelengths of the series of fully hydrated samples of mixed acid PC derivatives with one C_{18} chain and the other chain variable in length. All data were taken from heating scans.

PC	phase[a]	temperature range (°C)	bilayer repeat (nm)	ripple wavelength (nm)	monoclinic angle (°)	wide angle reflections (nm)
di-18:0	$L_{\beta'}$	<48.5	6.82			0.425, 0.408
	$P_{\beta'}$	48.5 to 57.0	6.99	16.76	97.35	0.425
	L_α	>57.0	6.79			0.457
18:0,16:0	$L_{\beta'}$	<33.1	6.61			0.419, 0.408
	$P_{\beta'}$	33.1 to 46.6	7.41	14.04	96.15	0.422
	L_α	>46.6	6.79			0.455
16:0,18:0	$L_{\beta'}$	<38.1	6.76			0.417
	$P_{\beta'}$	38.1 to 48.4	6.57	14.63	101.45	0.422
	L_α	>48.4	6.70			0.450
18:0,14:0	$L_{\beta'}$	<17.7	6.58			0.419, 0.408
	$P_{\beta'}$	17.7 to 32.2	6.13	12.61	98.1	0.425
	L_α	>32.2	6.01			0.457

[a]Diffraction measurements for the gel and liquid crystal phases were taken at temperatures in which the phase was stable. Ripple phase measurements were taken at the maximum value of the d_{01} peak.

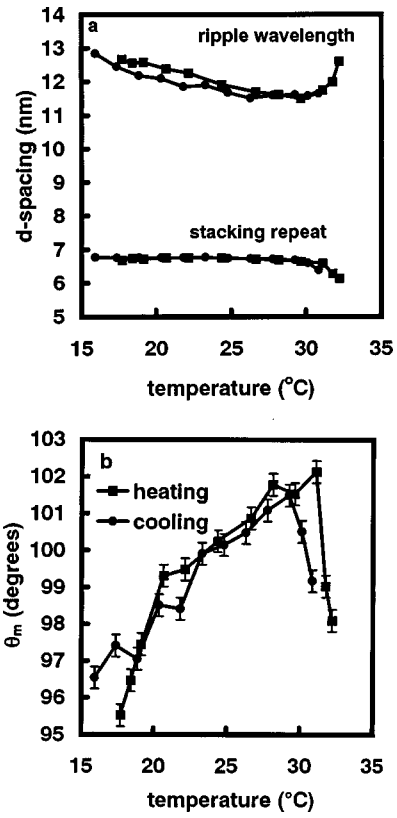

FIG. 4. Plots of the temperature dependence of (a) ripple wavelength λ and stacking repeat distance d_s and (b) the monoclinic angle θ_m, for fully hydrated 18:0,14:0 PC undergoing a heating scan (■) and a cooling scan (●). The scan rates were 2 °C/min.

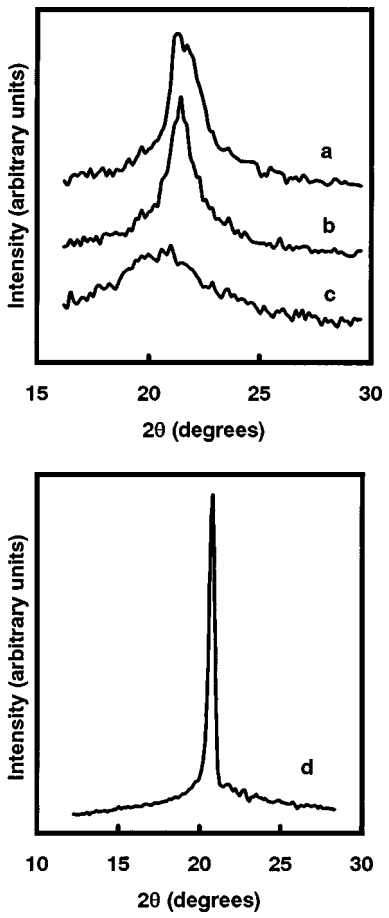

FIG. 5. WAXS diffraction patterns for (a) the $L_{\beta'}$, (b) the $P_{\beta'}$, (c) the L_α phases of fully hydrated 18:0,14:0 PC measured at 9.9, 21, and 33.4 °C, respectively, (d) the L_β phase of fully hydrated 16:0,18:0 PE measured at 13.5 °C.

$L_{\beta'}$ and L_α phases where λ tends to infinity.

On heating, θ_m initially increased rapidly from about 95.5 at 17.5 °C, the lowest temperature at which it could be reliably measured, to a value of about 99.5 at 20 °C and then more slowly to a maximum of about 102 at 30 °C [Fig. 4(b)]. On cooling, the behavior is very similar apart from a slight (1–2 °C) displacement of the curve to a lower temperature. θ_m would be expected to be 90° if the lipid chains were *either* all parallel to the normal to the layer plane *or* the average tilt in the two sections of the ripple were equal and opposite. This is likely to be the case only if the ripple phase is symmetric. The observed deviation in the value of θ_m from 90° strongly suggests that the ripple phase is inherently asymmetric. In general, θ_m would be expected to increase with increases in the disparity between ϕ_1 and ϕ_2, the angle of tilt with respect to the bilayer normal in the two ripple sections. Given the relatively small changes in value of λ, this might be expected to be reflected in an increase in ripple amplitude. This is consistent with the scanning-tunneling microscopy results of Woodward and Zasadzinski [18] showing that the ripple is inherently asymmetric and that its amplitude increases steadily with temperature before falling rapidly back towards zero as the system enters the planar L_α phase. The value of d_s remains almost constant at 6.7 nm throughout the ripple phase [Fig. 4(a)] suggesting that ripple asymmetry and amplitude have little effect on the average bilayer and interbilayer water thicknesses.

Typical WAXS diffraction patterns for the different phases of 18:0,14:0 PC seen in the gray-scale SAXS pattern shown in Fig. 3 are presented in Figs. 5(a)–5(c). A pattern for the untilted L_β phase of 16:0,18:0 PE is shown in Fig. 5(d) for comparison purposes. The pattern for the low-temperature phase [Fig. 5(a)] consists of a relatively sharp peak centered at $2\theta = 21.18°$ ($d = 0.419$ nm) with a shoulder at $2\theta = 21.76°$ ($d = 0.408$ nm). This type of pattern, as shown by Tardieu *et al.* [10], is typical of an $L_{\beta'}$ phase and corresponds to a quasihexagonal lattice in which the acyl chains are tilted with respect to the bilayer normal forming one group of four closely spaced chains with two chains at a slightly larger separation. The WAXS pattern for the $P_{\beta'}$ phase [Fig. 5(b)] consists of a single peak again centered at $d = 0.419$ nm. This peak is symmetrical indicating that the lipid chains are packed on a regular hexagonal lattice. It is, however, considerably broader than the corresponding peak of conventional L_β phases formed in planar bilayers [cf., Figs. 5(b) and 5(d)], reflecting the tilt of the chains in the $P_{\beta'}$ phase. The pattern for the L_α phase [Fig. 5(c)], as would be expected, consists of a single broad diffuse reflection.

Ripple phase formation in unsaturated molecular species. Verkleij *et al.* [4] and Ververgaert *et al.* [5] have reported freeze-fracture evidence for the formation of ripple phases in 18:1,18:0 PC and 16:0,18:1 PC. The formation of a ripple phase in unsaturated PC derivatives has, however, largely been ignored, probably as the result of a general failure to find evidence for a pretransition in these lipids using DSC

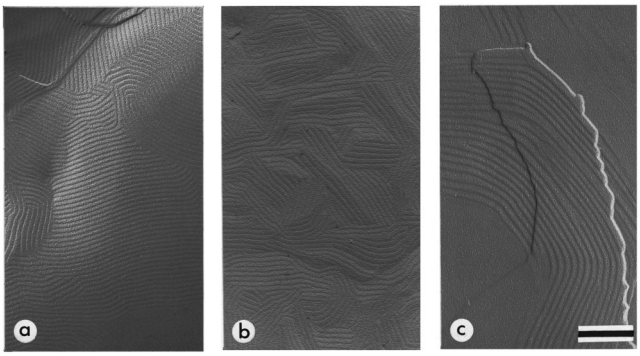

FIG. 6. Typical freeze-fracture electronmicrographs showing the pretransition ripples of (a) 18:0,18:1 PC, (b) 18:0,18:2 PC thermally quenched from 5 and −26 °C, respectively, and (c) 18:0,18:1 PC thermally quenched from −26 °C. The bar represents 200 nm.

techniques. We have confirmed the original freeze-fracture findings for 18:1,18:0 PC and, as illustrated in Fig. 6, also find clear evidence for ripple formation in 18:0,18:1 PC and 18:0,18:2 PC. In all cases the ripples appear to be standard asymmetric pretransition ripples of the type commonly seen for saturated PC derivatives. SAXS diffraction patterns of ripple phases formed by 18:0,18:1 PC, 18:1,18:0 PC, and 18:0,18:2 PC are presented in Fig. 7. Values for λ, d_s, and θ_m for these lipids are listed, together with the corresponding phase transition temperatures, in Table III.

Transition temperatures were normally measured using heating scans as marked hysteresis was observed in the cooling scans. This is illustrated for a partially hydrated sample of 18:0,18:1 PC in the SAXS measurements presented in Fig. 8(a). In this sample, the characteristic (0,1) diffraction maximum is clearly observable down to temperatures of at least −55 °C. On reheating the ripple phase first anneals out to yield an L_β phase. It then reforms when the sample reaches its normal ($L_\beta - P_{\beta'}$) transition temperature as shown in Fig. 8(b). The transition temperatures cited in Table III, it should be emphasized, were measured on fully hydrated samples of the lipids where hysteresis is less of a problem and the transition between the L_β and $P_{\beta'}$ phases is much more clear-cut. Hysteresis still occurs, however, as illustrated in the freeze-fracture electron micrograph showing the presence of this ''locked-in'' ripple phase in a sample of fully hydrated 18:0,18:1 PC thermally quenched from −26 °C shown in Fig. 6(c).

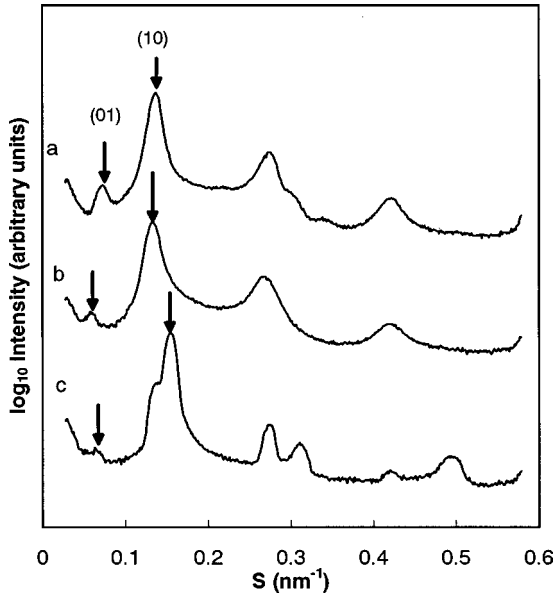

FIG. 7. SAXS diffraction patterns exhibiting the ripple phase in fully hydrated samples of unsaturated PC derivatives (a) 18:0,18:1 PC at 2.0 °C, (b) 18:1,18:0 PC at 7.5 °C, and (c) 18:0,18:2 PC at −19.1 °C. The positions of the (01) and (10) maxima are indicated by arrows (cf. Fig. 2).

In the case of 18:0,18:2 PC, ripple phase formation occurs at −17.2 °C. This is several degrees below the freezing point of ice in our x-ray samples even though they are prone to supercooling. This lipid undergoes a further transition to a gel phase at −28 °C. In contrast to the other unsaturated lipids, 18:0,18:2 PC appears to transform directly from the gel phase back into the L_α phase on reheating without passing through an identifiable ripple phase. This probably reflects freeze-dehydration effects that are much more severe at these low temperatures.

Formation of long-wavelength ripples. The presence of symmetric ripples with a wavelength about twice that of the normal pretransition ripples associated with the $P_{\beta'}$ phase has been widely reported in freeze-fracture studies performed on lipid mixtures containing PC derivatives [29,54–58]. Related structures, some symmetric and some asymmetric, have also been reported to occur as minor components in pure PC samples [25,26]. Apart from the report of Yao *et al.* [19] of the presence of *secondary ripples* in di-16:0 PC, the existence of long-wavelength ripple phases does not appear to have been observed in x-ray diffraction studies on pure PC samples.

We found little evidence for the existence of long-wavelength ripples in the x-ray diffraction patterns of most of the fully hydrated lipids that we examined. A clear reflection at very low angles was, however, observed, in a sample of 18:0,16:0 PC (lipid/water 1:0.5 w/w) freshly cooled from the L_α phase. Diffraction patterns showing this reflection are presented in Fig. 9. The upper diffraction pattern in this figure shows a reflection at $S = 0.0725\ \text{nm}^{-1}$ ($d = 13.7$ nm) corresponding to the (01) spacing of the conventional pretransition ripple and a reflection at $S = 0.0396\ \text{nm}^{-1}$ ($d = 25.3$ nm) that we attribute to the (01) spacing of the secondary ripple. As the sample was cooled, the reflection associated with the pretransition ripple reduced in intensity while that from the long-wavelength secondary ripple increased. Below about 28 °C, the reflection from the pretransition ripple disappeared and the long-wavelength ripple reflection broadened and shifted to a limiting spacing of $S = 0.0269\ \text{nm}^{-1}$ ($d = 37.2$ nm), yielding the diffraction pattern shown in the lower trace in Fig. 9. On reheating, the spacing associated with the pretransition ripple reappeared and there was again clear evidence for the coexistence of the two ripple forms. The wavelengths of the two ripple phases varied with temperature but their ratio remained close to 1.8:1 suggesting that they were closely related.

No sign of this long-wavelength spacing was observed in the initial heating scan of the sample suggesting that these longer-wavelength ripples are specifically formed as the sample cooled from the L_α phase. The intensity of the (01) spacing of the pretransition ripple on cooling is always much

TABLE III. Wide-angle diffraction spacings, bilayer repeat spacing, and ripple wavelengths of the series of fully hydrated samples of mixed acid PC derivatives with one C_{18} chain and the other chain variable in saturation. All data were taken from heating scans (except where indicated).

PC	phase[a]	temperature range (°C)	bilayer repeat (nm)	ripple wavelength (nm)	monoclinic angle (°)	wide angle reflections (nm)
18:0,18:1	L_β	<-1.3	6.44			0.419
	$P_{\beta'}$	-1.3 to 3.9	6.86	15.98	100.8	0.425
	L_α	>3.9	6.66			0.444
18:1,18:0	L_β	<1.2	6.47			0.422
	$P_{\beta'}$	1.2 to 7.5	7.38	15.29[c]		0.428
	L_α	>7.5	6.86			0.434
18:0,18:2[b]	L_β	<-28.2	6.48			0.419
	$P_{\beta'}$	-28.2 to -19.1	7.31	15.99	93.5	0.425
	L_α	>-19.1	6.34			0.434

[a]Diffraction measurements for the gel and liquid crystal phases were taken at temperatures in which the phase was stable. Ripple phase measurements were taken at the maximum value of the d_{01} peak.

[b]Diffraction measurements for 18:0,18:2 PC were taken during a cooling scan. The ripple phase forms only during cooling.

[c]We were unable to determine accurately the ripple wavelength and monoclinic angle for this lipid. The value reported is the (01) peak.

lower than the corresponding peak in the initial heating scan indicating a high degree of sample disorder. It is possible that conditions favorable to the formation of these longer-wavelength ripples, which we suspect to be identical to the secondary ripple reported by Yao *et al.* [19], exist in the freshly cooled samples but that such ripples anneal out on prolonged equilibration at lower temperatures.

Freeze-fracture replicas prepared from samples of this lipid thermally quenched from the pretransition range (30–40 °C), directly following cooling from the L_α phase, are dominated by the presence of standard pretransition ripples with a wavelength of about 13.3 nm, as shown in Fig. 10(a). Corresponding replicas quenched from temperatures below the transition range are characterized by large areas of planar bilayer arising from an $L_{\beta'}$ phase lipid together with smaller areas of long-wavelength ripple. Two distinct types of long-wavelength ripples were seen in such replicas. One type, shown in Fig. 10(b), had a similar asymmetric cross section to pretransition ripples but is of longer wavelength and is much more variable and nonuniform in appearance. This type appears simply to correspond to collapsing pretransition ripples.

The other type, shown in Fig. 10(c), was symmetrical in cross section and much more uniform in wavelength. It is almost certainly this more uniform type of ripple that corresponds to the secondary ripples detected by x-ray diffraction. The amounts, and the distribution of this type of ripple in

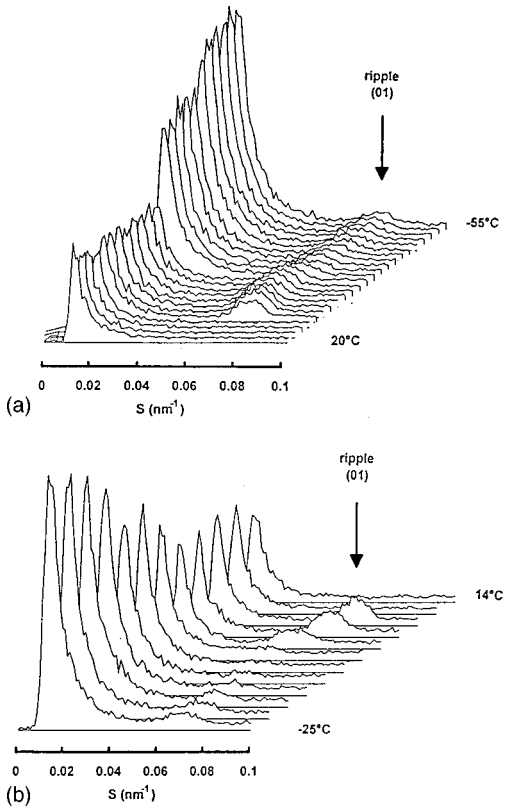

FIG. 8. Three-dimensional plot of a series of SAXS diffraction patterns for a sample of fully hydrated 18:1,18:0 PC (a) during cooling, (b) on reheating. Temperature scan rates were 5 °C/min.

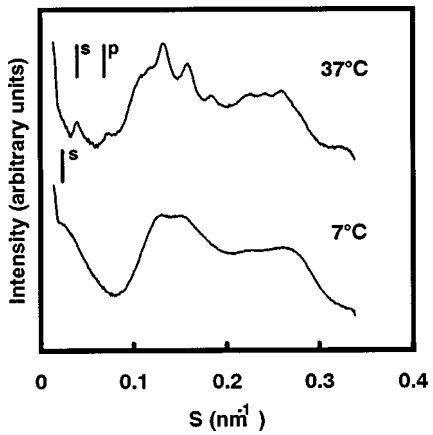

FIG. 9. SAXS diffraction patterns of a partially hydrated (33 wt. %) sample of 18:0,16:0 PC showing (a) both the pretransition (*p*) and secondary ripple (*s*) diffraction maxima and (b) the maxima corresponding to the secondary ripple and $L_{\beta'}$ phase. Measurements were made at 37 and 7 °C in the course of a cooling scan at 5 °C/min.

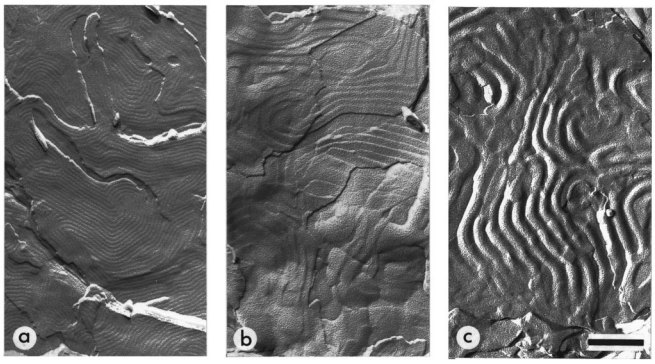

FIG. 10. Typical freeze-fracture electronmicrographs showing (a) the pretransition ripples of 18:0,16:0 PC in a sample thermally quenched from 37 °C and (b) and (c) two types of longer wavelength ripples seen in samples thermally quenched from 15 °C. The bar represents 200 nm.

different samples, appear to be very dependent on the thermal history of the samples in a way that it is still unclear, accounting for its apparent elusiveness in x-ray diffraction studies.

DISCUSSION

The three main areas investigated in this study are the effect of changes in the length, saturation, and position of the acyl chain on the occurrence and temperature range of the ripple phase; the formation and molecular organization of the ripple phase; and the relationship between pretransition and long-wavelength ripple phases.

Effects of chain length, position, and saturation. Cevc [45] has developed a simple model to describe the ripple phase based on the idea that ripple phase formation involves a mutual sliding of the acyl chains of the lipids along their long axes that is driven by an increase in headgroup hydration. Using this model he has shown that T_m and T_p, the temperatures of the $(L_{\beta'} \rightarrow P_{\beta'})$ and $(P_{\beta'} \rightarrow L_{\alpha})$ phase transitions, respectively, of saturated homoacyl PC derivatives, fit the following simple phenomenological equations:

$$T_m = 400(1 - 1.8/n_c - 25.2n_c^2), \tag{2}$$

$$T_p = 414(1 - 2.8/n_c - 21.5n_c^2), \tag{3}$$

where n_c is their chain length. A plot showing the fit of published values for a series of such derivatives to these equations is shown in Fig. 11. The corresponding values for the PC derivatives studied in this investigation, have been fitted to this plot on the basis of their T_m values. The chain length of the *equivalent* homoacyl saturated lipid can then be read directly from the plot.

In a related analysis of the dependence of T_m in monounsaturated PC derivatives on the double bond position [9], it is shown that their gel phases are principally stabilized by van der Waals interactions between the upper saturated parts of the chains, that chain-chain interaction in the disordered region(s) containing *cis*-double bond(s) is minimal, and that contributions of the shorter saturated tail sections of the lipids to gel-phase stability are relatively small. In the cases of the three saturated mixed chain-length derivatives studied here, all have equivalent n_c values slightly greater than the length of their shorter chain but appreciably less than that of their longer chain. This is consistent with the view that T_m is largely determined by chain-chain binding between the ordered sections common to both the *sn*-1 and *sn*-2 chains. The unsaturated lipids have much lower equivalent n_c varying from close to 12.5 for 18:0,18:1 and 18:1,18:0 PC to close to 11.1 for 18:0,18:2 PC, again consistent with the findings of Cevc [9].

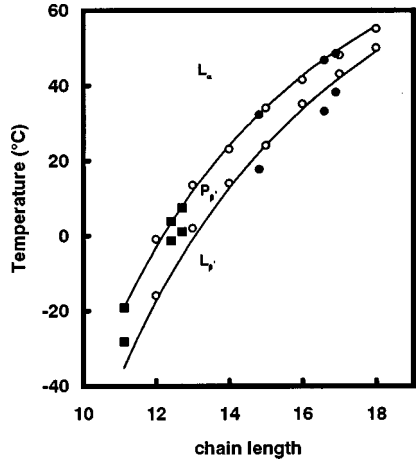

FIG. 11. Plot showing the dependence of the values of T_m and T_p of different PC derivatives as a function of chain length. The upper and lower curves are based on published T_m and T_p values for a series of homo di-acyl C_{12} to C_{18} PC derivatives (○) taken from Wack and Webb (1989), respectively. The corresponding values for the mixed chain saturated derivatives 18:0,14:0 PC, 18:0,16:0 PC, and 16:0,18:0 PC (●) and the unsaturated derivatives 18:0,18:1 PC, 18:0,18:2 PC, and 18:1,18:0 PC (■) examined in this study are fitted to the plot on the basis of their T_m values to indicate their effective overall chain lengths.

The values for the temperature span of the ripple phase $(T_m\text{-}T_p)$ of these two groups of lipids are plotted against their equivalent chain length in Fig. 12. The derivatives with two saturated chains of different length show larger pretran-

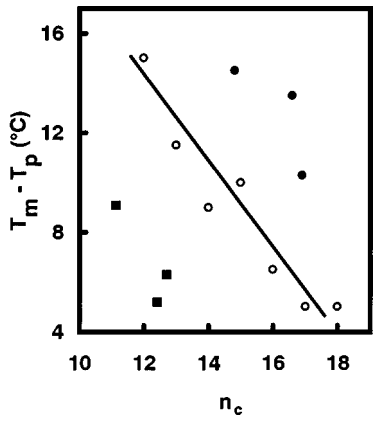

FIG. 12. Plot of $T_m\text{-}T_p$ values as a function of chain length for the series of homo di-acyl C_{12} to C_{18} PC derivatives (○). The corresponding values for the mixed chain saturated derivatives 18:0,14:0 PC, 18:0,16:0 PC, and 16:0,18:0 PC (●) and the unsaturated derivatives 18:0,18:1 PC, 18:0,18:2 PC and 18:1,18:0 PC (■), plotted as a function of their effective overall chain lengths as estimated from Fig. 11, are included for comparison purposes.

sition temperature spans than their equivalent homoacyl saturated lipids while those containing unsaturated chains are characterized by smaller spans. These differences can readily be explained, at a qualitative level at least, in terms of the sliding chain model. As the chains of the homacyl saturated lipids slide past each other on formation of the ripple phase, there is a loss of chain-chain interaction reflecting a reduction in the length of overlapping regions of ordered chains in neighboring lipids. In the case of the saturated mixed-chain derivatives, in contrast, as the acyl chains slide past each other, the previously disordered tail sections of the longer chains are now available to line up alongside the ordered chains of neighboring lipids. The activation energy required to initiate chain sliding is thus lower and the threshold temperature for such motion is reduced. Conversely, in the case of lipids containing disruptive *cis*-double bonds, chain sliding leads to these bonds being drawn up into a previously ordered region resulting in a greater than normal disruption of chain-chain interactions. The activation energy for chain sliding is correspondingly higher and the threshold temperature is raised.

Formation and molecular organization of the ripple phase. The driving force for formation of the ripple phase according to the Cevc model is headgroup hydration associated with an increase in exposure to the aqueous phase. This increased exposure of the headgroup tends to lead to an increase in the cross-sectional area of the headgroup putting the cohesive chain-chain interactions under stress. This imbalance between the forces acting in the headgroup and acyl chain regions is similar, but acting in an opposite manner, to that invoked by Gruner [59] and Tate and Gruner [60] in their explanation of the phase behavior of H_{II} lipids. In the H_{II}-forming lipids, where the headgroups occupy less area than their acyl chains, it tends to separate the two monolayers imposing a negative curvature on the monolayers leading to the formation of cylindrical inverted micelles. In the PC system, the opposing monolayers will tend to bend in the opposite direction in an attempt to form the corresponding micellar system. This, however, is prevented by the relative incompressibility of the lipid acyl chains. The imbalance between the expansive forces associated with increased headgroup hydration and the cohesive forces associated with chain-chain interactions within the bilayer appears to be most easily relieved by a buckling of the bilayer to form the ripple phase. If the lipid molecules were perfectly cylindrically symmetric, this buckling would be expected to be sinusoidal with no preferred axis with respect to the plane of the bilayer. In practice, lipid molecules are inherently asymmetric giving rise to a ripple phase.

Electron density profile calculations performed by Wack and Webb [16] show that the pretransition ripple phase $P_{\beta'}$, in agreement with electron microscopy studies, is asymmetric with a sawtooth profile. The precise interpretation of the organization of the lipid molecules within this sawtooth is, however, still uncertain. These workers estimated an average value of 34°–41° for ϕ', the average tilt angle *with respect to the normal of the average layer line*, for the ripple phases of di-C_{12} through to di-C_{19} PC. This analysis was based on a comparison of the measurements of projected chain area, on the average layer plane of the bilayer with the corresponding calculated values for the fully extended chains oriented parallel to the bilayer normal. As they point out, it is difficult to be sure in such measurements whether the values obtained for ϕ' are a true reflection of the average tilt of the chains with respect to the bilayer or simply reflections of the algaebraic sum of the contributions of the bilayer thicknesses of gel and liquid-crystal phase components present in the ripple phase. They concluded, on the basis of measurements of the incremental change in the value of d_1' with chain length, that chain tilt was the major contribution to their value for ϕ'. The inference of this is that the physical state of the lipids is similar throughout the ripple profile.

Sun *et al.* [20] have recently reported calculations of the electron density profiles of the ripple phase of di-14:0 PC based on the same data but using a different modeling approach. Their calculations confirm the sawtooth profile but predict that its two segments are quite different in organization. The major segment was found to have a head-to-head bilayer thickness of 3.79 nm, very similar to the value of 3.7 nm found for the gel phase, while that of the minor section was found to be 3.1 nm, more typical of the L_α phase.

If correct, the ripple might be expected to be equivalent to a mixture of gel and liquid-crystal phase lipid in the approximate proportions of the lengths of the two sides. This corresponds to approximately 70% gel and 30% liquid-crystal phase. If there is approximately 30% liquid-crystal phase lipid in the ripple phase, this might be expected to be detectable in the WAXS diffraction pattern. Typical patterns for the $P_{\beta'}$ and L_α phases of 18:0,14:0 PC are shown in Fig. 13(a). The difference pattern obtained by subtraction of 30% of the pattern of the L_α phase from that of the $P_{\beta'}$ phase as a whole is shown in Fig. 13(b). This pattern, which might be expected to correspond to the contribution of the major side of the sawtooth, is clearly different from that of the total pattern for the $P_{\beta'}$ phase but is still of a shape consistent with the idea that the gel phase can be represented as a tilted set of hexagonally packed rods along the lines suggested by Tardieu *et al.* [10]. The model suggested by Sun *et al.* [20] is thus at least reconcilable with our WAXS data.

Relationship between pretransition and long-wavelength ripple phases. Although there is still room for disagreement on the analysis of the precise electron density profile of the ripple phase, there appears to be little doubt that the standard pretransition ripple is an asymmetric sawtooth structure. This conclusion is fully supported by freeze-fracture [25,26] and tunneling electron microscopy studies [28]. The situation regarding long-wavelength ripple phases is less clear-cut. In our studies, we observe two distinct long-wavelength forms. One of these is clearly asymmetric and closely resembles the pretransition ripple [cf., Figs. 10(a) and 10(b)]. It is commonly observed in samples of saturated PC derivatives that have been recently cooled below their normal ($L_{\beta'}$-$P_{\beta'}$) phase transition temperatures. This form, which is somewhat variable in wavelength, does not give rise to an x-ray diffraction peak and appears simply to reflect the presence of pretransition ripple phases that have not reequilibrated with the bulk phase. The other, less common, form is symmetrical in profile [Fig. 10(c)]. It appears to be related to the pretransition ripple in that x-ray diffraction measurements indicate that the ratio of the wavelengths of the two types of ripples is fixed in their coexistence range.

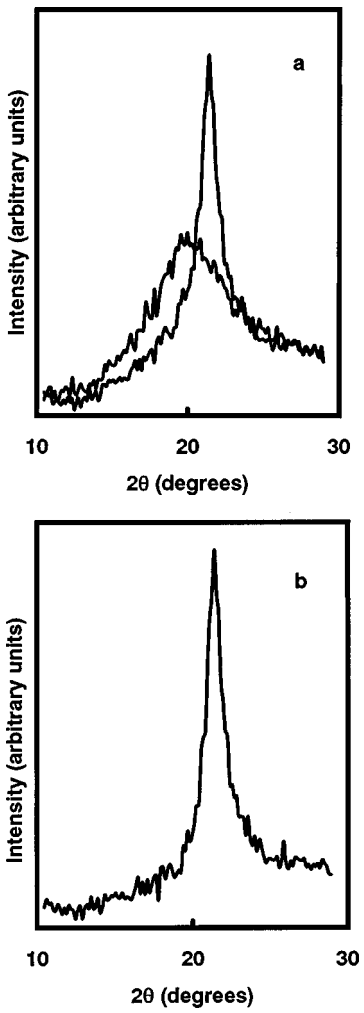

FIG. 13. Comparison of (a) the measured WAXS diffraction patterns of the $P_{\beta'}$ and L_{α} phases of 18:0,14:0 PC and (b) the pattern calculated by subtraction of 30% of the pattern for the L_{α} phase from that of the $P_{\beta'}$ phase.

The nature and origin of these symmetrical ripples is not fully clear. They appear to form as the lipid cools from the L_{α} phase. On cooling from the L_{α} phase, pretransition ripples with mutually different orientations will inevitably be formed simultaneously in different parts of the bilayer. These will propagate towards each other and it is perhaps not surprising that unusual ripple profiles will be generated in their intersecting regions. With this in mind, the idea put forward by Meyer that symmetrical ripples may be based on two opposing sections of tilted gel phase, each of which is similar in organization to the long side of the sawtooth pretransition ripple, seems to be particularly worthy of careful consideration. It is noteworthy in this context that by virtue of its tilted chains, the $L_{\beta'}$ phase has an in-built directionality, possibly explaining why these more complex ripple forms are not normally observed on heating equilibrated gel phase samples.

CONCLUSION

This study has explored the dependence of the ripple phase on unsaturation and length of the acyl chain in phosphatidylcholines. We found that the temperature dependency of the ripple wavelength, stacking repeat, and monoclinic angle defining the unit cell are consistent with an asymmetric ripple having an amplitude that slowly increases with temperature. The ripple asymmetry and amplitude appear to have little effect on the average bilayer and interbilayer water thickness. The WAXS data are consistent with the model suggested by Sun *et al.* [20], in which the minor side of the ripple sawtooth has gel-like properties and the major side of the ripple sawtooth has liquid crystal-like properties. A further investigation of the acyl chain packing may help elucidate the characteristics of the acyl chains in each section of the ripple phase sawtooth structure.

The temperature spans of the ripple phases of saturated mixed-chain PC derivatives were found to be larger than those of homoacyl derivatives of the same equivalent length. In contrast, the temperature spans of the ripple phases of PC derivatives containing unsaturated chains were found to be smaller than those of the equivalent homoacyl derivatives. This is consistent with a model involving a mutual sliding of the acyl chains along their long axes that is driven by an increase in headgroup hydration suggested by Cevc [45]. The activation energy for chain sliding is reduced for saturated chains due to an ordering of the tail sections of the longer chains resulting in a lowering of the threshold temperature, whereas the activation energy is increased for unsaturated chains due to the disruptive *cis*-double bonds resulting in an increase in the threshold temperature.

A variety of secondary ripples are produced in phospholipids depending on sample preparation and thermal history. A secondary ripple phase with a wavelength of about 1.8 times greater than the conventional pretransition ripple phase was observed in our samples. These ripples are symmetric in cross section, form only on cooling from the L_{α} phase, and persist to much lower temperatures than the pretransition ripple. The symmetric ripples may form when two opposing sections of tilted gel phase merge as suggested by Meyer [26]. Further investigation of these secondary ripples, both symmetric and asymmetric, may reveal the nature of their production as well as the nature of the production of the pretransition ripple.

ACKNOWLEDGMENTS

The support of the ESPRC and the technical assistance of the staff of SRS, Daresbury are gratefully acknowledged.

[1] M. J. Ruocco and G. G. Shipley, Biochim. Biophys. Acta **691**, 309 (1982).

[2] E. N. Serrallach, G. H. de Haas, and G. G. Shipley, Biochemistry **23**, 713 (1984).

[3] J. Mattai, P. K. Sripada, and G. G. Shipley, Biochemistry **26**, 3287 (1987).

[4] A. Verkleij, P. Ververgaert, L. Van Deenen, and P. Elbers, Biochim. Biophys. Acta **288**, 326 (1972).

[5] P. Ververgaert, A. Verkleij, P. Elbers, and L Van Deenen, Biochim. Biophys. Acta **311**, 320 (1973).
[6] K. Mortensen, W. Pfeiffer, E. Sackmann, and W. Knoll, Biochim. Biophys. Acta **945**, 221 (1988).
[7] D. Wolfe, L. J. Lis, O. Kucuk, M. P. Westerman, B. A. Cunningham, W. Bras, and P. J. Quinn, Phys. Rev. Lett. **68**, 1085 (1992).
[8] A. Watts, K. Harlos, W. Maschke, and D. Marsh, Biochim. Biophys. Acta **510**, 63 (1978).
[9] G. Cevc, Biochim. Biophys. Acta **1062**, 59 (1991).
[10] A. Tardieu, V. Luzzati, and F. C. Reman, J. Mol. Biol. **75**, 711 (1973).
[11] M. J. Janiak, D. M. Small, and G. G. Shipley, Biochemistry **15**, 4575 (1976).
[12] M. J. Janiak, D. M. Small, and G. G. Shipley, J. Biol. Chem. **254**, 6078 (1979).
[13] J. Stamatoff, H. J. Feuer, G. Guggenheim, G. Tellez, and T. Yamane, Biophys. J. **38**, 217 (1982).
[14] M. R. Alecio, A. Miller, and A. Watts, Biochim. Biophys. Acta **815**, 139 (1985).
[15] B. Tenchov, H. Yao, and I. Hatta, Biophys. J. **56**, 757 (1989).
[16] D. C. Wack and W. W. Webb, Phys. Rev. A **40**, 2712 (1989).
[17] S. Matuoka, S. Kato, M. Akiyama, Y. Amemiya, and I. Hatta, Biochim. Biophys. Acta **1028**, 103 (1990).
[18] S. Matuoka, S. Kato, and I. Hatta, Biophys. J. **67**, 728 (1994).
[19] H. Yao, S. Matuoka, B. Tenchov, and I. Hatta, Biophys. J. **59**, 252 (1991).
[20] W.-J. Sun, S. Tristram-Nagle, R. M. Suter, and J. F. Nagle, Proc. Natl. Acad. Sci. USA **93**, 7008 (1996).
[21] P. Pinta da Silva, J. Microsc. **12**, 185 (1971).
[22] E. J. Luna and H. M. McConnell, Biochim. Biophys. Acta **466**, 381 (1977).
[23] R. Krbecek, C. Gebhardt, H. Gruler, and E. Sackmann, Biochim. Biophys. Acta **554**, 1 (1979).
[24] A. Hicks, M. Dinda, and M. A. Singer, Biochim. Biophys. Acta **903**, 177 (1987).
[25] J. A. N. Zasadzinski, Biochim. Biophys. Acta **946**, 235 (1988).
[26] H. W. Meyer, Biochim. Biophys. Acta **1302**, 138 (1996).
[27] J. A. N. Zasadzinski, J. Scheir, J. Gurley, V. Elings, and P. K. Hansma, Science **239**, 1013 (1988).
[28] J. T. Woodward and J. A. Zasadzinski, Biophys. J. **72**, 964 (1997).
[29] H. W. Meyer, B. Dobner, and K. Semmler, Chem. Phys. Lipids **82**, 179 (1996).
[30] We have used the following abbreviations for lipids in this study: di-14:0 PC, 1,2 myristoyl-*sn*-glycero-3-phosphocholine; di-18:0 PC, 1,2 stearoyl-*sn*-glycero-3-phosphocholine; 18:0,16:0 PC, 1-stearloyl-2-palmitoyl-*sn*-glycero-3-phosphocholine; 16:0,18:0, 1-palmitoyl-2-stearoyl-*sn*-glycero-3-phosphocholine; 18:0,14:0 PC, 1-stearoyl-2-myristoyl-*sn*-glycero-3-phosphocholine; 18:0,18:1 PC, 1-stearoyl-2-oleoyl-*sn*-glycero-3-phosphocholine; 18:1,18:0 PC, 1-oleoyl-2-stearoyl-*sn*-glycero-3-phosphocholine; 18:0,18:2 PC, 1-stearoyl-2-linoleoyl-*sn*-glycero-3-phosphocholine.
[31] S. Doniach, J. Chem. Phys. **70**, 4587 (1979).
[32] M. S. Falkovitz, M. Seul, H. L. Frisch, and H. M. McConnell, Proc. Natl. Acad. Sci. USA **79**, 3918 (1982).
[33] M. Marder, H. L. Frisch, H. S. Langer, and H. M. McConnell, Proc. Natl. Acad. Sci. USA **81**, 6559 (1984).
[34] J. M. Carlson and J. P. Sethna, Phys. Rev. A **36**, 3359 (1987).
[35] R. E. Goldstein and S. Leibler, Phys. Rev. Lett. **61**, 2213 (1988).
[36] T. C. Lubensky and F. C. MacKintosh, Phys. Rev. Lett. **71**, 1565 (1993).
[37] C. M. Chen, T. C. Lubensky, and F. C. MacKintosh, Phys. Rev. E **51**, 504 (1995).
[38] P. A. Pearce and H. L. Scott, J. Chem. Phys. **77**, 951 (1982).
[39] A. Georgallas and M. J. Zuckerman, Eur. Biophys. J. **14**, 53 (1986).
[40] M. H. Hawton and W. J. Keeler, Phys. Rev. A **33**, 333 (1986).
[41] H. L. Scott and P. A. Pearce, Biophys. J. **55**, 339 (1989).
[42] W. S. McCullough and H. L. Scott, Phys. Rev. Lett. **65**, 931 (1990).
[43] W. S. McCullough, J. H. H. Perk, and H. L. Scott, J. Chem. Phys. **93**, 6070 (1990).
[44] H. L. Scott and W. S. McCullough, Int. J. Mod. Phys. B **15**, 2479 (1991).
[45] G. Cevc, Biochemistry **30**, 7186 (1991).
[46] B. Cunningham, L. J. Lis, P. J. Quinn, and W. Bras, J. Biochem. Biophys. Methods **29**, 87 (1994).
[47] W. P. Williams, B. A. Cunningham, D. H. Wolfe, G. E. Derbyshire, G. R. Mant, and W. Bras, Biochim. Biophys. Acta **1284**, 86 (1996).
[48] L. G. Dowell, S. W. Moline, and A. P. Rinfret, Biochim. Biophys. Acta **59**, 229 (1962).
[49] W. P. Williams, A. P. R. Brain, B. A. Cunningham, and D. H. Wolfe, Biochim. Biophys. Acta **1326**, 103 (1997).
[50] H. Lin, Z. Wang, and C. Huang, Biochemistry **29**, 7063 (1990).
[51] T. Bultmann, H. Lin, Z. Wang, and C. Huang, Biochemistry **30**, 7194 (1991).
[52] P. J. Davis, B. D. Fleming, K. P. Coolbear, and K. M. W. Keough, Biochemistry **20**, 3633 (1981).
[53] K. P. Coolbear, C. B. Berde, and K. M. W. Keough, Biochemistry **22**, 1466 (1981).
[54] C. Gebhadt, H. Gruler, and E. Sackmann, Z. Naturforsch. C **32**, 581 (1977).
[55] B. R. Copeland and H. M. McConnell, Biochim. Biophys. Acta **599**, 95 (1980).
[56] S. K. Malhotra, S. Ross, and J. P. Tewari, Chem. Phys. Lipids **28**, 33 (1981).
[57] T. Endo, K. Inoue, S. Nojima, T. Sekiya, K. Ohki, and Y. Nozawa, J. Biochem. **93**, 1 (1983).
[58] R. E. Brown, W. H. Anderson, and V. S. Kulkarni, Biophys. J. **68**, 1396 (1995).
[59] S. Gruner, Proc. Natl. Acad. Sci. USA **82**, 3665 (1985).
[60] M. W. Tate and S. M. Gruner, Biochemistry **28**, 4245 (1989).